Tellus (2007), 59B, 412–424
Printed in Singapore. All rights reserved

TELLUS

High resolution modelling of atmosphere-canopy exchange of acidifying and eutrophying components and carbon dioxide for European forests

By G. PIETERSE[1]*, A. BLEEKER[1], A. T. VERMEULEN[1], Y. WU[2] and J. W. ERISMAN[1],
Energy Research Institute of the Netherlands, Westerduinweg 3, 1755 ZG Petten, The Netherlands;
Hydrological Sciences Branch, NASA Goddard Space Flight Center, Greenbelt, Maryland, USA

(Manuscript received 28 April 2006; in final form 4 December 2006)

ABSTRACT

The Integrated Deposition Model (IDEM) was improved by incorporating a novel multilayer biochemical dry deposition module for gases. The aerosol and base cation deposition module was adopted from IDEM. For evaluation of primary and ecosystem productivity, carbon respiration schemes were included. The resulting Framework for Atmosphere-Canopy Exchange Modelling (FACEM) was then evaluated by the case studies presented here. First, results for deposition of SO_x, NO_y and NH_x were compared with site observations, showing correlations of up to $R^2 = 0.60$. Applicability for grid deposition calculations for these compounds was then evaluated for Europe. The model was clearly able to reproduce the elevated deposition near the important emission areas in Europe. Next, we compared the modelled CO_2 fluxes with measurements from 26 European sites. Correlations of up to $R^2 = 0.81$ indicate good performance. To evaluate grid performance, the 2003 European heat wave was studied in a final case study, resulting in convincing correspondence with the observed productivity anomalies.

1. Introduction

The development of practical models that are able to reproduce site-level observations remains a challenging issue for atmospheric modellers. Atmospheric deposition for instance is determined by many physical and chemical processes that take place simultaneously on a large range of temporal and spatial scales. One other related challenge is that deposition modelling involves many fields of expertise. Much effort has been put into performing measurements for different vegetation types and species (e.g. Bennet et al., 1973; Wesely, 1989; Hicks et al., 1991; Erisman and Draaijers, 1995; Katul et al., 1996; Meyers et al., 1998; Pleim et al., 1999). Also, many theories and models have been developed, describing the driving mechanisms for the physical, chemical and biological processes. Another important area of related research is the development of biosphere-atmosphere exchange models in which many sub model scale processes described by these theories have been incorporated (e.g. Running and Coughlan, 1988; Potter et al., 1993; Sellers et al., 1996; Adiku et al., 2006). By doing so, a large amount of sometimes poorly verifiable parameters are introduced, resulting in a possible accumulation of uncertainties. The computational efforts required to run the comprehensive models are very often considerable, rendering these models impractical for usage in impact studies. This paper introduces a first version of the Framework for Atmosphere-Canopy Exchange Modelling (FACEM). This framework consists of a combination of mechanistic and empirical sub models. We choose to incorporate mechanical models only when the underlying processes are considered sufficiently well understood and when it is expected that such models will actually improve overall accuracy. In all other cases measurements are used, if available. Furthermore, high computational efficiency is required as the ultimate goal is to develop a framework suitable for impact studies involving a large number of simulations. Section 2 describes of the original model from which FACEM was developed. The implemented improvements are described in Section 3. The model-to-measurement comparisons are discussed in Section 4 and summarized in Section 5 and 6.

*Corresponding author.
e-mail: g.pieterse@phys.uu.nl
Present affiliation: Institute for Marine and Atmospheric Research Utrecht (IMAU), Princetonplein 5, 3584 CC Utrecht, The Netherlands.
DOI: 10.1111/j.1600-0889.2007.00266.x

2. Model description

The Integrated dry Deposition Model (IDEM) framework (Bleeker et al., 2004; Erisman et al., 2004; Gauger et al., 2003) is an inferential scheme, which evolved from the model for European Deposition of Acidifying Components on a small Scale

(EDACS: van Pul et al., 1995) and contains a module for calculating dry Deposition of Acidifying Components (DEPAC: Erisman et al., 1994). In inferential models (e.g. Garland, 1977; Hicks et al., 1991) the deposition flux F_c^i of a certain chemical species i to the surface is calculated as the product of the measured—or modelled—difference between the ambient and surface concentration (C_a^i and C_0^i, respectively) and the deposition velocity of the observed species, v_d^i:

$$F_c^i = v_d^i \left(C_a^i - C_0^i\right). \tag{1}$$

The different right hand side terms of this equation are explained in the following sections.

2.1. *Deposition velocity*

The deposition velocity is derived from a multiple-resistance transfer model consisting of a single (big leaf) or a multilayer representation of the surface layer. The different processes are represented by a chain of resistances including: (i) the aerodynamic resistance R_a. This resistance accounts for the turbulent diffusion in the surface layer, (ii) the boundary-layer resistance R_b. This resistance accounts for the molecular diffusion through the layer just above the surface layer, and finally, (iii) the surface resistance R_s which describes the processes taking place at the surface. Within a canopy, the surface resistance is strongly influenced by the photosynthetic response of the canopy to ambient conditions and restrictions, which is modelled by the leaf stomatal resistance R_{st}.

The single layer IDEM model uses the stomatal resistance scheme described by Baldocchi et al. (1987). Furthermore, IDEM uses empirical functions for the remaining resistances, e.g. the cuticle resistance, R_c. These empirical functions have been established by many micro meteorological, concentration and deposition flux measurements at forest and cropland sites. The approach is to first determine the aerodynamic and boundary-layer resistances, and thereafter deduce the surface resistance from the deposition flux equation (eq. 1) and the observed deposition flux. The surface resistance is specified per vegetation type and for a range of environmental conditions.

The multilayer BioChemical (MLBC) model (Wu et al., 2003b) uses a mechanical multilayer model for photosynthesis (Berry and Farquhar, 1978; Collatz et al., 1991) to calculate the stomatal resistance, and a passive membrane transport model for calculation of the cuticle resistance. The photosynthesis scheme provides a full description of the stomatal resistance coupled to the biochemical mechanisms governing photosynthesis and also considers the (coupled) effects of environmental conditions. The multilayer approach allows for a more adequate treatment of the nonlinear transport of radiation through the canopy.

In FACEM, we have replaced the single layer IDEM model by the more sophisticated MLBC model. By adding this more generic approach we expect to obtain a framework which is generally applicable to deposition calculations at high temporal and spatial resolution. Recent studies (Meyers et al., 1998; Wu et al., 2003b) confirm that the multilayer approach improves deposition model performance. Furthermore, the biochemical scheme for photosynthesis provides an opportunity for extension towards a more generic approach for the species of interest, enabling combined evaluation of nitrogen, sulphur as well as carbon fluxes. The model-to-measurement comparisons for the carbon fluxes presented in this work required us to incorporate carbon respiration schemes. These schemes will also enable future comparisons with results from other models and are described in more detail in Section 3.2.

2.2. *Background and surface concentrations*

The surface layer is very often considered to be a perfect sink for depositing species and that therefore the surface concentration can be set to zero. However, several studies show that this assumption is in some cases invalid for NH_3. For example, Farquhar et al. (1980) showed that nitrogen metabolism can produce NH_3. In that case, C_0 may even exceed C_a, resulting in emission rather than deposition of NH_3 (Sutton et al., 1996). Dry deposition is also reversible for most gas species and it can therefore be expected that for some cases the surface layer will act as source rather than a sink. This means that for these cases, the surface concentration cannot be set to zero. In this study, we consider the case for the reemission of NH_3 only.

Equation 1 implies that the deposition of a certain species i is not influenced by the deposition and presence of other species. However, for example in the case of simultaneous deposition of SO_2 and NH_3, e.g. Erisman and Wyers, (1993) found mutually dependent deposition fluxes and incorporated a correction for co-deposition of SO_2 and NH_3 DEPAC. This parameterization is adopted for FACEM.

The presence of water on leaf surfaces influences the surface chemistry and thereby the co-deposition of SO_2 and NH_3. Several studies (e.g. Garland, 1977; Fowler and Unsworth, 1979; Fowler, 1985; Schuepp, 1989; Erisman and Wyers, 1993; Flechard et al., 1999; Finkelstein et al., 2000; Wu et al., 2003b) show that SO_2 deposition depends on humidity and temperature. Although potentially important, we do not account for the temperature and humidity dependence of co-deposition.

3. Model framework development

First, the MLBC and the DEPAC deposition modules were integrated. The original MLBC model is applicable for site-level calculations only. Local meteorological conditions, the vegetation Leaf Area Index (LAI) and the Available Soil Water (ASW) must be measured and used for input. To reduce the dependency on the availability of measurements, the input requirements were adapted for meteorological data from the European Center of Medium-range Weather Forecasts (ECMWF). For the purpose of studying the carbon cycle, simple carbon respiration schemes were added to the biochemical photosynthesis scheme provided by the MLBC model. The following sections describe the integration of the two deposition modules (Section 3.1), incorporation of the respiration schemes (Section 3.2) and finally the required general framework improvements (Section 3.3).

3.1. *Integration of DEPAC and MLBC deposition modules*

The original MLBC model is only applicable for gaseous species whereas DEPAC is applicable for gaseous and as particulate deposition. Therefore, two classes of species were considered for the development of FACEM, namely: (i) gaseous species; including SO_2, O_3, HNO_3, NO, NO_2 and NH_3, (ii) and particles; including SO_4, NO_3, NH_4 and base cations. The CO_2 and H_2O fluxes are calculated in the stomatal resistance scheme of the MLBC model. Wu et al. (2003b) show that the model results for CO_2, H_2O, O_3 and SO_2 agree well with the measurements performed at several sites. A parameterization for HNO_3 is also implemented in the original MLBC model, however the authors did not evaluate the performance for this species. For the development of FACEM, NO_2, NO and NH_3 were also added. DEPAC contains a scheme for cases in which the leaf surface acts as a source for NH_3 and this model furthermore accounts for co-deposition of NH_3 and SO_2. Both approaches were adopted for this study. Finally, the single layer base cation deposition scheme of the DEPAC model was adopted for FACEM.

3.2. *Addition of respiration schemes*

The MLBC model describes photosynthesis as this is a driving mechanism for the opening and closure of leaf stomata and the corresponding exchange of CO_2 and water vapour. As a result, the MLBC model provides estimates for Gross Primary Productivity (GPP), the uptake of CO_2 due to photosynthesis. However, this quantity is difficult to measure directly because other processes are at the same time (and place) responsible for (re)emission of CO_2. The fluxes resulting from these respiration processes are divided into two groups: autotrophic and heterotrophic respiration (R_{auto} and R_h). R_{auto} is the carbon that is re-emitted as a result of plant growth and tissue maintenance. R_h is the amount of carbon that is emitted due to microbial activity in the carbon pools within the soil and vegetation litter layers. Quantities that are more often measured, are the Net Primary Productivity (NPP) and the Net Ecosystem Productivity (NEP). The NPP is calculated as GPP-R_{auto} and subsequently, NEP is calculated as NPP-R_h. Simple autotrophic and heterotrophic respiration modules were implemented in FACEM to allow for validation of NPP and NEP, and herewith indirectly the GPP estimates obtained by the model calculations.

3.2.1. Autotrophic respiration. Autotrophic respiration consists of maintenance and growth respiration, R_m and R_g, respectively. The former is estimated by a scheme adopted from an algorithm used to produce MODIS NPP products (Heinsch et al., 2003). This algorithm is based on the assumption that the maximum sustainable leaf biomass is linked to the amount of live-wood and fine-roots. In this approach, the leaf mass at a certain time t is calculated using the following expression:

$$M_l = \frac{LAI\,(t)}{SLA}, \tag{2}$$

where SLA is the specific leaf area, which is a vegetation-dependent constant given for different types of vegetation in Table 1. The following expressions are used to calculate the live-wood and fine-root maintenance respiration, R_m^{lw} or R_m^{fr} respectively:

$$R_m^i = M_i R_{m,20}^i Q_{10}^{a\,\frac{T-20.0}{10.0}},\ i = [lw, fr] \tag{3}$$

where Q_{10}^a is the vegetation-dependent Arrhenius ratio and $R_{m,20}^i$ is the maintenance respiration at 20°C for plant compartment i, again shown in Table 1. The live-wood and fine-root biomass (M_{lw} and M_{fr}) are calculated using the following expression:

$$M_i = r_i^l M_{l,max}.\ i = [lw, fr] \tag{4}$$

Table 1. Land cover classification and vegetation-dependent model parameters

Vegetation type	Height m	Profile –	SLA m^2kg^{-1}	Q_{10}^a –	f_{fr}^l –	f_{lw}^l –	$R_{m,20}^{fr}$ $kgCm^{-2}d^{-1}$	$R_{m,20}^{lw}$ $kgm^{-2}d^{-1}$	$R_{h,15}^{ll}$ $kgm^{-2}yr^{-1}$	$R_{h,15}^{hl}$ $kgm^{-2}yr^{-1}$
Deciduous broad leaf	23.0	2	32.2	2.0	1.1	0.203	0.00519	0.00371	0.047	0.026
Evergreen broad leaf	16.0	2	20.3	2.0	1.1	0.162	0.00519	0.00397	0.042	0.026
Evergreen needle	23.0	2	16.1	2.0	1.3	0.081	0.00519	0.00322	0.049	0.032
C_3 crops	0.5	1	40.0	2.0	2.0	0.000	0.00619	0.00000	0.050	0.037
C_3 grasses	0.5	1	40.0	2.0	1.0	0.000	0.00519	0.00000	0.042	0.031
C_4 crops	0.5	1	40.0	2.0	2.0	0.000	0.00619	0.00000	0.050	0.037
C_4 grasses	0.5	1	40.0	2.0	1.0	0.000	0.00519	0.00000	0.042	0.031
Shrubs	0.5	1	18.0	2.0	1.4	0.079	0.00519	0.00436	0.038	0.032

In this equation, $M_{l,max}$ is the maximum leaf biomass during the growing season, calculated using eq. 2. The factor r_i^l is the vegetation-dependent ratio between leaf biomass and the biomass in plant compartment i, representing either the live-wood or the fine-root compartment (see Table 1). The leaf maintenance respiration R_m^l is calculated in the stomatal resistance scheme (Collatz et al., 1991, 1992) and depends on the photosynthetic pathway:

$$R_m^l = \begin{cases} 0.015 V_{max}, & \text{for } C_3 \text{ plants} \\ 0.025 V_{max} & \text{for } C_4 \text{ plants} \end{cases} \quad (5)$$

Here, V_{max} is the maximum catalytic capacity of Rubisco, an enzyme required to catalyze the first important reaction in carbon fixation. Following the approach used by Knorr (2000), the growth respiration is then calculated as follows:

$$R_g = f_g(\text{GPP} - R_m - R_g). \quad (6)$$

The factor f_g is an empirical factor equal to 0.25. The GPP is provided by the stomatal resistance scheme adopted from the MLBC model. Now, NPP can be calculated using the following expression:

$$\text{NPP} = \text{GPP} - R_m - R_g, \quad (7)$$

where R_m is the sum of all maintenance respiration processes and R_g is the growth respiration.

3.2.2. Heterotrophic respiration. A heterotrophic respiration scheme is required for estimating the NEP. Heterotrophic respiration is generally considered to be linearly dependent on soil carbon content. Many biosphere models (e.g. Running and Coughlan, 1988) therefore use long term spin-up runs to build up a soil carbon pool, based on the modelled history of vegetation growth and mortality. For FACEM, we have used the soil carbon data from the IGBP-DIS database (see Section 3.3.5.), which is derived from many measurements. This was partly for practical reasons. However, incorporating a mechanistic scheme to build up a soil carbon pool requires numerous schemes for biological and soil transport processes to be included, herewith introducing a large amount of new parameters with significant uncertainty. The question is whether this is desirable. On a yearly basis, heterotrophic respiration will decrease the soil carbon pool by only a few percent (Ito and Oikawa, 2000). Furthermore, the soil carbon pool will be replenished by litter fall and biomass mortality. The total amount of carbon in the soil is generally two to three orders of magnitudes larger than the heterotrophic respiration fluxes and therefore. Therefore, we assume that the error introduced by neglecting the carbon pool variability is small compared to the uncertainties introduced by the parameters in the expressions for heterotrophic respiration from the litter and humus layer, R_h^{ll} and R_h^{hl} (Ito and Oikawa, 2000; Aurora, 2003)

$$R_h^i = R_{h,15}^i C_i f_{15} g_i. \; i = [ll, hl] \quad (8)$$

Here, $R_{h,15}^i$ is the vegetation-dependent respiration rate at 15 °C (see Table 1) and C_i the soil carbon pool for soil compartment i, obtained from the IGBP-DIS dataset. The factor f_{15} is given by

$$f_{15} = Q_{10}^{h\,\frac{(T-15.0)}{10.0}}, \quad (9)$$

where Q_{10}^h is assumed to be dependent on the soil temperature (T) and is given by the following expression:

$$Q_{10}^h = e^{2.04\left(1-\frac{T}{T_{opt}}\right)}. \quad (10)$$

The optimum temperature (T_{opt}) for heterotrophic respiration is set equal to 36.9 °C. For the humus layer, the factor g_{hl} in eq. 8 is provided by the following expression:

$$g_{hl} = \begin{cases} 1 - 0.5\frac{ln(\psi)-ln(\psi_{sat})}{ln(0.04)-ln(\psi_{sat})}, & 0.04 \geq \psi > \psi_{sat} \\ 1, & 0.06 \geq \psi \geq 0.04 \\ 1 - \frac{ln(\psi)-ln(0.06)}{ln(100.0)-ln(0.06)}, & 100.0 \geq \psi > 0.06 \\ 0. & \psi > 100.0 \end{cases} \quad (11)$$

In this expression, ψ is the soil water tension, given by

$$\psi = \psi_{sat}\left(\frac{\theta}{\theta_{sat}}\right)^{-c}. \quad (12)$$

The parameters ψ_{sat} and θ_{sat} (the saturated soil moisture content, expressed in terms of soil water tension and content, respectively) and c are related to the soil type. For the litter layer, the factor g_{ll} is calculated using an expression similar to eq. 11. In this case, we assume that the heterotrophic respiration from the litter layer is not limited by high moisture content (or low soil water tension). For this study, the amount of carbon in the litter layer was set to 1% of the total amount of carbon in the soil. The approximation for heterotrophic respiration can be used to obtain NEP from NPP using eq. 7 introduced in the previous section:

$$\text{NEP} = \text{NPP} - R_h, \quad (13)$$

where R_h is the sum of all heterotrophic respiration processes.

3.3. Improved model input

3.3.1. Implementation of meteorological data. The original IDEM model uses ECMWF meteorological data and this approach was used for the development of FACEM. For the case studies presented in Section 4, we have used data with a spatial resolution of 1° for the years 2000–2003. The original temporal resolution of the ECMWF data was 3, hr and we have linearly interpolated these data to a temporal resolution of 1, hr. The data are not readily applicable for FACEM model calculations because the ECMWF model has its own roughness length parameterization. At a specific site, the ECMWF modelled roughness length $z_{0,E}$ generally differs significantly from the site-level roughness length z_0 and displacement heigh (D) calculated by the model of Massman (1997). Using the ECMWF wind fields for the surface layer, without accounting for the effect of the local roughness length, would therefore lead to over or underestimation of the wind speed required for calculation of the aerodynamic and boundary-layer resistances. The wind fields are therefore corrected using the local roughness length and displacement height. This correction is performed in FACEM by following an approach introduced by Wieringa (1986). First, the ECMWF wind speed U_E at a certain height z in the surface layer is scaled to the wind speed U_b at the blending height z_b. At this height, the effects of all surface inhomogeneities are assumed to be blended into the mean flow. The wind speed at the blending height is calculated using the following expression:

$$U_b = U_E \frac{ln\left(\frac{z_b - z_{0,E}}{z_{0,E}}\right) - \Psi_m\left(\frac{z_b}{L}, \frac{z_{0,E}}{L}\right)}{ln\left(\frac{z - z_{0,E}}{z_{0,E}}\right) - \Psi_m\left(\frac{z}{L}, \frac{z_{0,E}}{L}\right)}. \quad (14)$$

This equation is derived from the standard definition of the surface layer (e.g. Stull, 1988; Liu et al., 1979). The same expression is then used to scale the wind speed at the blending height back to the original height, but this time by using the local roughness length z_0 and displacement height D:

$$U = U_b \frac{ln\left(\frac{z - D - z_0}{z_0}\right) - \Psi_m\left(\frac{z-D}{L}, \frac{z_0}{L}\right)}{ln\left(\frac{z_b - D - z_0}{z_0}\right) - \Psi_m\left(\frac{z_b - D}{L}, \frac{z_0}{L}\right)}. \quad (15)$$

The ψ-functions from ?) were taken from the MLBC model. In this approach, it is assumed that the Monin-Obukhov length L, obtained from ECMWF, is applicable for both expressions. Strictly speaking, this assumption is invalid because eq. 15 requires the site-level Monin-Obukhov length. However, the error introduced by this assumption will generally be less than the error made without compensating for local roughness, provided that the two following criteria are met: (i) the blending height is chosen to conform with the length scale of the major surface inhomogeneity. Apart from being dependent on the atmospheric stability, the blending height is a function of the horizontal scale of the surface heterogeneity (Mason, 1988; Claussen, 1990; Mahrt et al., 1998; Philip, 1997; Ma and Daggupaty, 1998; Verkaik, 2000), and (ii) the local velocity U is calculated at approximately the same effective height ($z - D$) as the height z from which U_E was obtained. In FACEM, the blending height is set to $60 + D$ meters. In case of zero displacement height, this corresponds with a surface inhomogeneity scale of several hundreds of meters. After correction of the wind speed, the local turbulence parameters such as the friction velocity and the Monin-Obukhov length are re-evaluated.

3.3.2. Implementation of concentration data. The concentration data required for FACEM is calculated by the Danish Eulerian Hemispheric Model (DEHM) and was provided by NERI, Denmark (Christensen, 1997; Frohn et al., 2002, 2003; Geels, 2003; Geels et al., 2004). The concentration data is available at a spatial resolution of 0.5° and a time resolution of 3 hr. The DEHM model uses emission inventory data at a resolution of 50 km to produce concentration fields for many components, including SO_2, SO_4, NO, NO_2, NO_3, HNO_3, NH_3 and NH_4, the species of interest in this study.

3.3.3. Implementation of the land cover dataset. Recently, the SYNMAP (Jung et al., 2006) land cover dataset has become available to the scientific community. This synergistic global dataset provides land cover data with spatial resolutions of up to 1km and has been derived from the Global Land Cover Characteristics dataset (GLCC: Loveland et al., 2000), the global land cover classification for the year 2000 (GLC2000: Joint Research Centre., 2003), the MODIS MODIS land cover product (Friedl et al., 2002) and continuous tree cover data provided by the Advanced Very High Resolution Radiometer (AVHRR). One of the main reasons for choosing this land cover dataset is that it is partly derived from the MODIS land cover product and MODIS satellite observations are required as an important input for calculations with FACEM (see Section 3.3.4.). The fact that several other high-resolution global land cover datasets were joined to obtain SYNMAP (Jung et al., 2006), was also considered to be potentially advantageous for future comparison studies. For this work, the SYNMAP dataset was aggregated to a resolution of 0.25°, using the land cover classification scheme shown in Table 1 that summarizes the vegetation heights and the canopy structure profile indices (Massman, 1982; Wu et al., 2003a) assumed for the different land use classes. The results presented in Section 4 were obtained by assigning the dominant land cover type to each grid cell. Grid cells for which a dominant land cover type could not be determined were excluded. Future studies will include a fractionated approach because we expect this will improve the model performance significantly.

3.3.4. Implementation of MODIS dataset. The required LAI data in this study have been obtained from the MODIS dataset (Knyazikhin et al., 1999) because the MLBC model itself does not calculate vegetation growth. The monthly averaged LAI data used for this study however contain gaps. These gaps are mainly due to MODIS instrument and meteorological limitations, e.g. the presence of clouds. The gaps are filled by averaging all other LAI data for the same land cover type in the 2° latitudinal band surrounding the individual site. If no LAI data is available for a certain month and latitudinal band, then LAI data available for the remaining months is interpolated using linear spline interpolation (Press et al., 1992).

3.3.5. Implementation of IGBP-DIS dataset. The soil characteristics required for the water stress model implemented in the photosynthesis scheme of the MLBC model (Wu et al., 1989), were obtained from the IGBP Data Information System (IGBP-DIS: Global Soil Data Task Group., 2000). This dataset provides soil structure data in terms of percentages sand and clay. These classes are then transformed to match the classification implemented in the MLBC model (Schaap and Leij, 1998; Schaap et al., 2001). The data set also provides the soil carbon content data required for the heterotrophic respiration scheme introduced in Section 3.2.2 For this study, the IGBP-DIS dataset was aggregated to a spatial resolution of 0.25°.

4. Model evaluation by different case studies

We have tested the overall performance of the FACEM model using a set of different case studies. The results are shown in the following sections.

4.1. *Acidifying and eutrophying components*

4.1.1. Site-level calculations. The site-level deposition calculations were performed for Level II forest plots of the Integrated Cooperative Programme (ICP) of the Convention on Long-Range Trans boundary Air Pollution (CLRTAP). In this program, the Level I and Level II measurement network was established, enabling monitoring of forest conditions and their spatial and temporal changes in Europe. The Level I network consists of approximately 6000 monitoring sites for basic forest condition measurements, while there are more than 860 Level II sites for more extensive measurements. At 360 of these Level II sites, atmospheric deposition is measured. This dataset allows for evaluation of the FACEM deposition estimates. The deposition measurements at the Level II sites consist of throughfall, stemflow and bulk deposition measurements. These measurements can be used as an input for the Canopy Budget Model (CBM: Draaijers and Erisman, 1995), which yields estimates for total deposition to a forest. Although uncertainties in the resulting deposition estimates can be as large as 40% (e.g. Draaijers and Erisman, 1995; Draaijers et al., 1998), these estimates allow for some quantitative validation of the FACEM results. For the comparison, wet deposition estimates were added to the FACEM and IDEM dry deposition calculations. These wet deposition data were provided by the DEHM model, described in Section 3.3.2 We have chosen a subset of sites by matching the land use classifications in the Level II site descriptions and the classifications provided by the SYNMAP dataset. Sites for which the classifications did not match were excluded for the comparison, resulting in exclusion of about 60% of the sites, with 92 sites remaining. Figure 1 shows the distribution of these sites over Europe. We performed calculations for the year 2002 using FACEM and IDEM and compared the results for the total annual deposition of SO_x, NO_y and NH_x with the CBM deposition estimates for the selected sites. Table 2 shows the performance of FACEM and IDEM for this comparison, illustrating an improved correlation for SO_x($R^2 = 0.60$) for FACEM compared with IDEM ($R^2 = 0.45$). A slight improvement in correlation was also found for NH_x ($R^2 = 0.42$ instead of $R^2 = 0.34$), but especially in terms of the bias between the model results and the CBM deposition estimates (99 $molha^{-1}yr^{-1}$ instead of 217 $molha^{-1}yr^{-1}$). For NO_y, the results for both models are similar in terms of correlation ($R^2 = 0.35$). For both models, this poor correlation is accompanied with a significant underestimation of the variability compared with the CBM estimates. Considering the fact that both models yield comparable results but are using a very different approach to model the deposition, the poor performance could very well be explained by inconsistencies in the CBM estimates. However this discrepancy remains unsolved because no other dataset exists for further analysis.

Fig. 1. Distribution over Europe of the 92 Level II sites included in the comparison.

Table 2. Model-to-measurement comparison for the different components of the 92 European Level II sites included in the comparison

Component	Model	Results		
		R^2	σ	Bias
		–	[$molha^{-1}yr^{-1}$]	[$molha^{-1}yr^{-1}$]
SO_x	FACEM	0.60	113	30
	IDEM	0.45	130	19
	CBM	–	110	–
NO_y	FACEM	0.35	143	−58
	IDEM	0.35	155	−34
	CBM	–	258	–
NH_x	FACEM	0.42	435	99
	IDEM	0.34	491	217
	CBM	–	353	–

Since FACEM includes a mechanistic photosynthesis scheme for multiple layers, a scheme that requires additional data which are currently only scarcely available, we believe that this good comparison with a less demanding but well-validated model like IDEM is very promising for future applications. The introduction of the photosynthesis scheme will also allow for future applications in integrative studies for biosphere-atmosphere exchange of nitrogen, sulphur and carbon fluxes. FACEM is evidently adequate in reproducing the deposition estimates obtained using the CBM, given the fact that there are large uncertainties involved in both the measurements and (the parameters required for) the modelled processes.

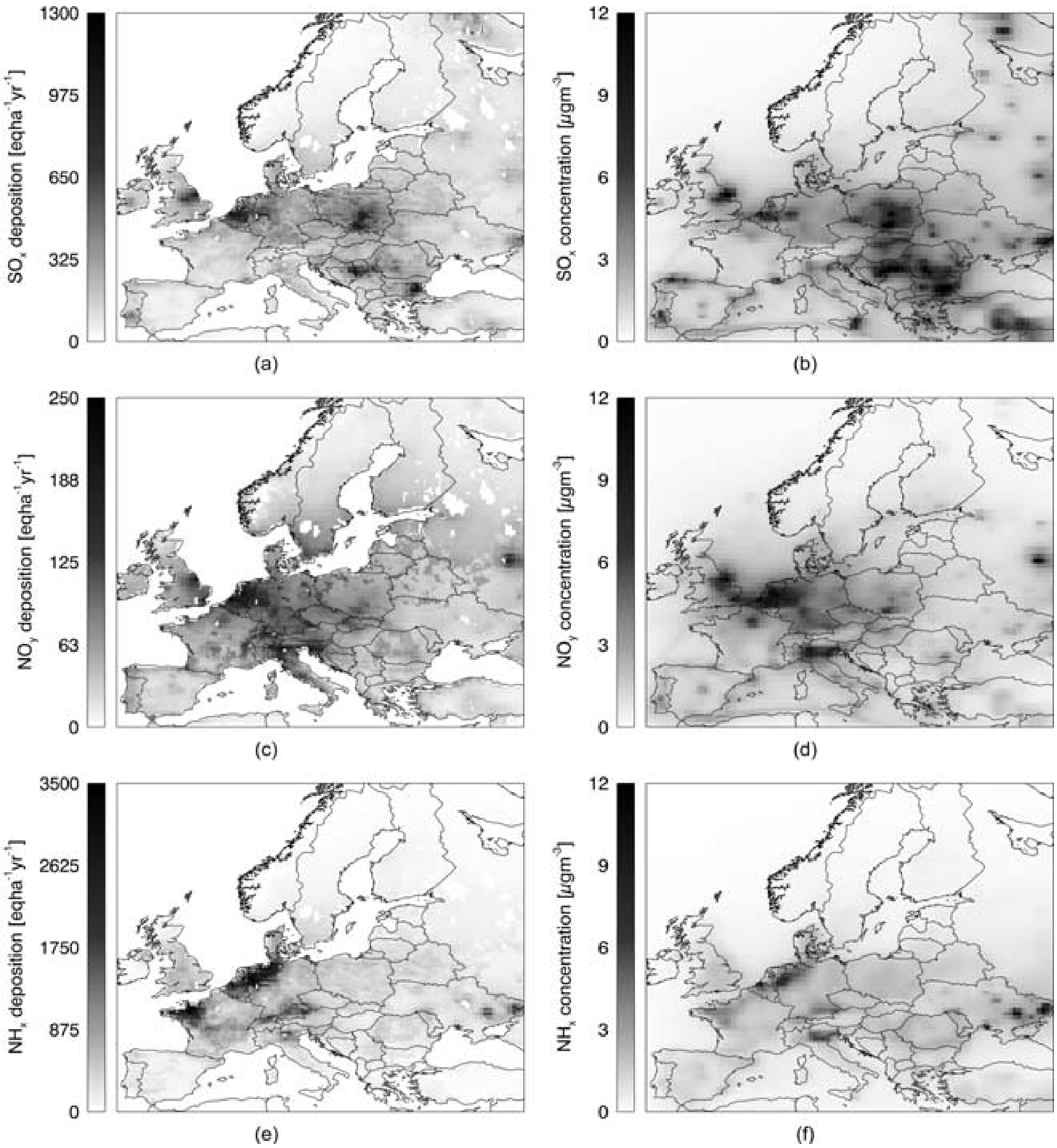

Fig. 2. Spatial distribution of annual deposition [eq ha^{-1}yr^{-1}] and yearly averaged background concentrations [μg m^{-3}] of (a, b) SO_x, (c, d) NO_y and (e, f) NH_x over Europe in 2002.

4.1.2. Grid-level calculations. Following the calculations for specific (forest) sites, a first grid-based calculation was performed for the European domain. These calculations required other data sources than those used for the site calculations (see Section 3.3) and were performed at a spatial resolution of 0.25° and a temporal resolution of 3 hr. Input data like monthly LAI, meteorological data and concentrations were interpolated to the output resolution of 0.25°. Figure 2 shows the modelled depositions for SO_x, NO_y and NH_x. Contrary to the site-level deposition data, the data shown here consists only of dry deposition; wet deposition is not included. The spatial distributions shown in Figure 2 are to a large extent governed by the distribution of the DEHM concentration data (see eq. 1). Due to the strong relation between the concentration fields and the emissions, the resulting deposition data clearly show the important emission areas in Europe with clear differences for the different components, shown by the distributions of the yearly averaged concentrations for SO_x, NO_y and NH_x also shown in Figure 2. Further research is required to gain more insight in the representativeness of the modelled deposition fluxes. After further validation of the data, model results like those presented here can be used for investigating deposition loads to different ecosystems and/or other receptors in relation to observed effects.

4.2. Carbon dioxide

4.2.1. Site-level calculations. In order to verify the CO_2 fluxes calculated by FACEM quantitatively, we have performed a

Fig. 3. Overview of 26 plots with different kinds of vegetation, used for site-level comparison with modelled CO_2 fluxes. DBF = deciduous boreal forest, EBF = evergreen boreal forest, ENF = evergreen needle forest, G = Grassland and MF = Mixed forest.

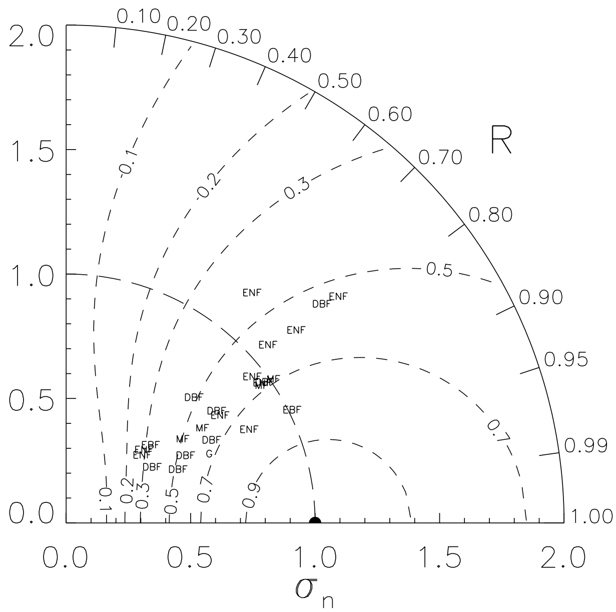

Fig. 4. Model performance in terms of correlation (R) and normalized standard deviation σ_n, compared with site-level CO_2 flux measurements during the summer months of 2000–2003 for 26 ICP plots with different kinds of vegetation. DBF = deciduous boreal forest, EBF = evergreen boreal forest, ENF = evergreen needle forest, G = Grassland and MF = Mixed forest.

site-level comparison with CO_2 flux measurements from 26 sites participating in the CarboEurope Integrated Project, see Figure 3. Grid-level calculations were performed for the summer months of 2000–2003, with a temporal resolution of 1 hr and a spatial resolution of 0.25°. The model results for the site-level measurements were obtained by extracting the results from the grid-cells of residence (Fig. 4). The model generally shows good correlations (up to $R^2 = 0.81$) with the measured values. In some cases, the variability is over or underestimated by 50%, which is illustrated by the normalized standard deviation σ_n in the figure. However, these kind of differences are not uncommon this kind of comparisons and as the order of magnitude of the modelled variability is approximately the same as the measured variability, we consider these results acceptable.

4.2.2. Grid-level calculations. As a case study for grid-level application, calculations were performed to study the GPP, NPP and NEP anomalies observed during the summer of 2003. The anomalies were caused by a period of high temperatures and severe draught during the summer of that year (Ciais et al., 2005). Because we expected that the effects of the draught on the vegetation would be visible in the MODIS LAI data and this information would actually force the model results towards the actual observations, we chose to apply the LAI data for the year 2002 for all summers of 2000 to 2003. We also used the same distribution of soil water content for the start of each summer period. This initialisation was based on the hydraulic characteristics of the different soil types. The 2003 anomaly was calculated as the difference between the average of each summer month of 2003 and the average of each summer month of 2000–2002. The results for July are presented in Fig. 5, in which the primary production anomalies are clearly visible. Ciais et al. (2005) found significant decreases in primary productivity for France, Italy, Romania and the Ukraine. The FACEM model results presented here agree well with these findings. Apparently, the high temperatures and severe draught in the summer of 2003 caused severe depletion of the available soil water in large regions of France, Italy and Romania. The extended Hadley cell responsible for the heat wave in the Southwestern part of Europe was also responsible for more rainfall and lower temperatures in the Northeastern part of Europe (e.g. in the Ukraine). This again resulted in a decrease in primary productivity. The results of the calculations with FACEM presented here confirm that lower or higher soil water availability, associated with respectively higher or lower temperatures were indeed the most important meteorological factors influencing the primary production anomalies during the summer of 2003. Interestingly, Fig. 5 shows a positive NEP anomaly in the Western part of Europe and that it is closely related to the available soil water. Whereas GPP and NPP are reduced, it appears that this reduction is partly, and in some cases completely compensated by a reduction of heterotrophic respiration, again due to low soil water availability (see eq. 11). Figure 6 shows the GPP anomaly obtained from the MOD17A2 product derived from MODIS satellite observations (Heinsch et al., 2003). These data show a more pronounced effect due to the heat wave than predicted by FACEM. Furthermore, the MOD17A2 data clearly show an increase of GPP in the Ukraine whereas a decrease is modelled by FACEM. Also, the model does not reproduce the strong increase in the GPP in the Southern part of Sweden although it appears that the observed anomaly is also less pronounced in this region than in other parts of Sweden. Of course, some discrepancies were expected because the simulations were performed using LAI data of the year 2002 for

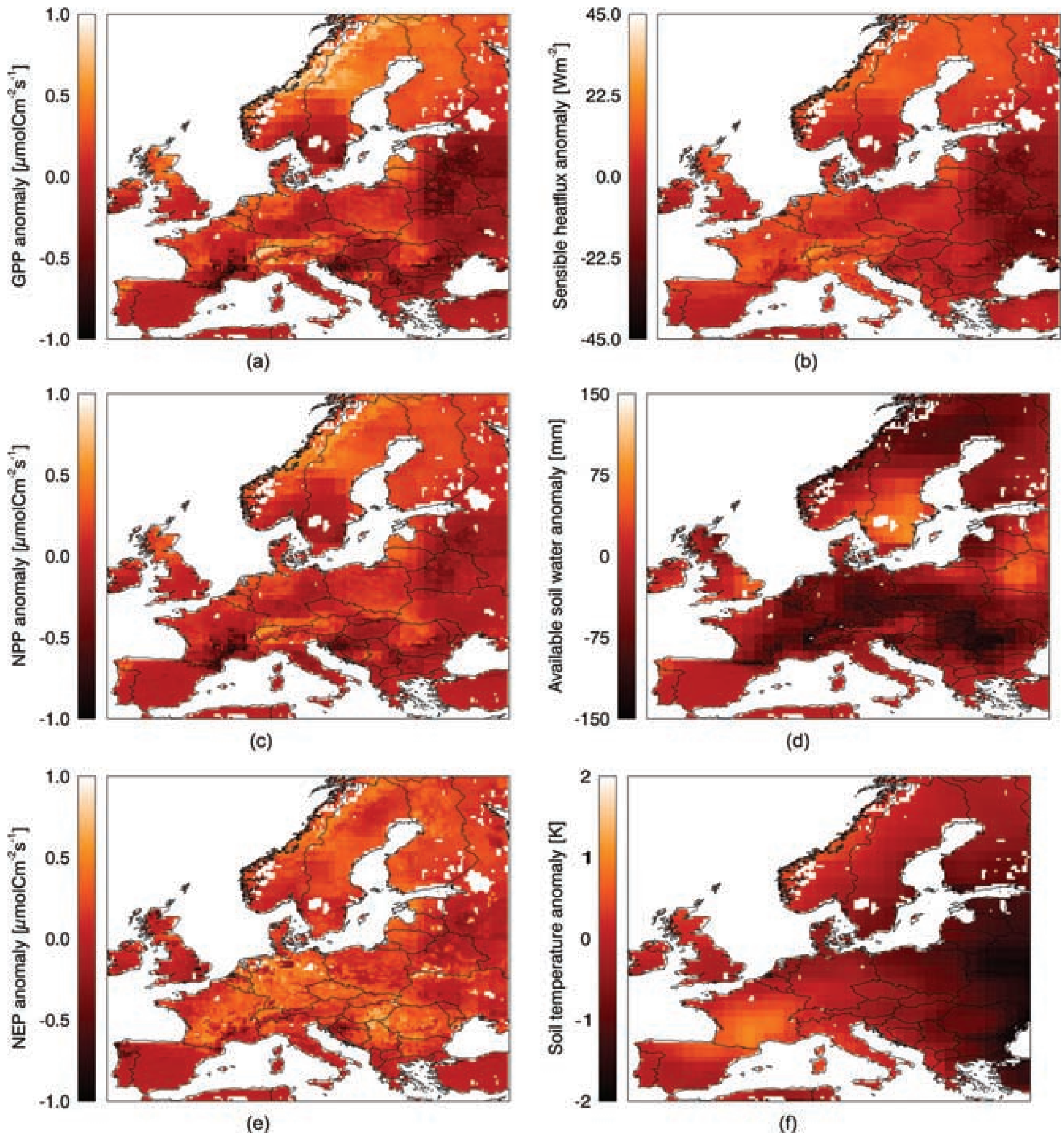

Fig. 5. Overview of results for 2003 anomaly for the (a) GPP anomaly [μmolCm^{-2}s^{-1}], (b) heat flux anomaly [Wm^{-2}], (c) NPP anomaly [μmolCm^{-2}s^{-1}], (d) available surface water anomaly [mm], (e) NEP anomaly [μmolCm^{-2}s^{-1}] and (d) soil temperature anomaly [K].

all years. Figure 7 shows the difference between the LAI observations for July 2002 and the observations for the same month in 2003. The observed LAI was either comparable or, especially for France, lower during July 2003, except for a region in the Ukraine near the black sea. For this region, this difference appears to be responsible for the difference between the modelled and observed GPP anomaly. For the other regions, this explains the more pronounced anomaly observed by MODIS. However, this statement does not hold for the southern part of Sweden. This could be caused by an overestimation of the available soil water and therefore inhibition of the photosynthesis by the model. On the other hand, a more detailed analysis of the data quality of the MOD17A2 GPP estimates shows that these estimates are less reliable for this region (see Fig. 8). Unfortunately, site-level measurements for this particular region were not available at the time of this study and therefore further analysis was not possible. Grid-based observations for net primary and ecosystem productivity are in general only scarcely available, if available at all. The MOD17A3 (Heinsch et al., 2003) NPP data, from which the FACEM respiration scheme was adopted, are available in the form of annual averages. However, the model calculations were performed for the summer months only and therefore a grid-based comparison was not possible for this case. Grid-based observations for the NEP were not available at the time of this study rendering a comparison impossible. However, the site-level results shown in the previous section were sampled from

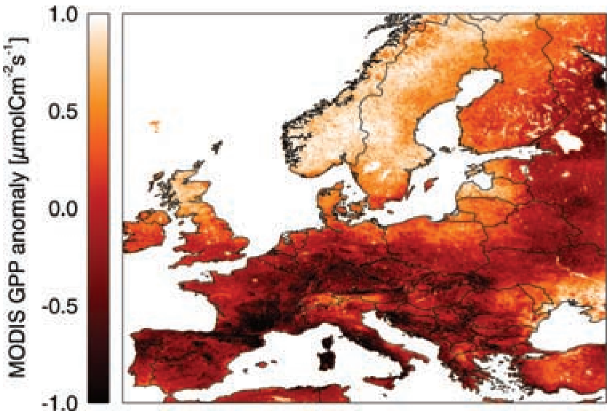

Fig. 6. Overview of results for the 2003 GPP anomaly [μmolCm^{-2}s^{-1}] provided by the MOD17A2 land algorithm (Heinsch et al., 2003) derived from MODIS satellite observations.

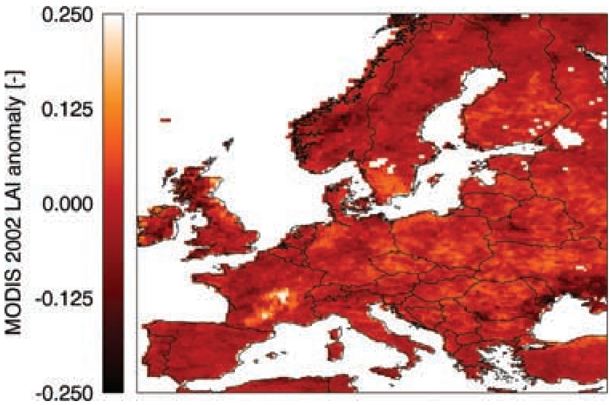

Fig. 7. Difference between MODIS satellite LAI observations for July 2002 and July 2003.

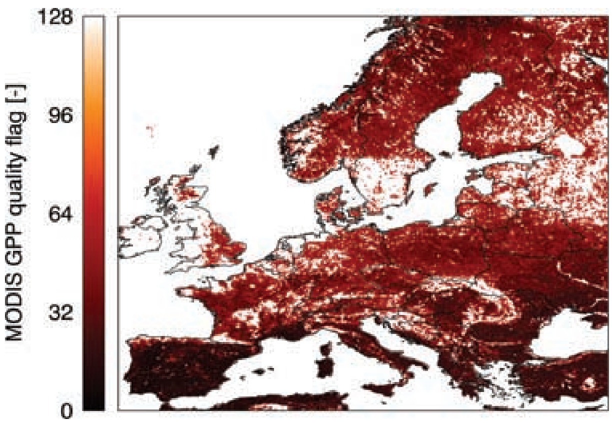

Fig. 8. Average values for the data quality flags for MOD17A2 GPP observations for the month July of the years 2000 to 2003. In this figure, poor data quality is represented by high values.

the grid-based calculations and can therefore be considered to be indicative for good grid-level performance.

5. Summary

In this work, the new FACEM was introduced and evaluated. In a first site-level comparison with CBM deposition estimates for 92 ICP forest plots, the model performance for deposition calculations was evaluated. In this comparison, the FACEM model results were also compared with the results obtained by the empirical IDEM model, from which the new model was partly derived. The model-to-measurement comparison should be seen in the light of the large uncertainties accompanying the CBM deposition estimates. These uncertainties were previously found to be as large as 40% (Draaijers and Erisman, 1995; Draaijers et al., 1998). Therefore, discrepancies between the modelled deposition fluxes and the CBM deposition estimates are also the result of the uncertainties in the CBM estimates. To avoid representation errors, the ICP descriptions for all ICP level II deposition measurement sites were compared with the SYNMAP dominant land cover classification. Sites with non-matching dominant land cover classifications were therefore excluded for the comparison. The FACEM model results showed an improved correlation for SO_x ($R^2 = 0.60$), as compared with the IDEM model ($R^2 = 0.45$). A slight improvement in correlation was also found for NH_x ($R^2 = 0.42$ instead of $R^2 = 0.34$), but especially in terms of the bias between the model results and the CBM deposition estimates (99 molha^{-1} yr^{-1} instead of 217 molha^{-1} yr^{-1}). In the second case study, a grid-based calculation was performed for the European domain. The results indicated that the FACEM model is able to reproduce the expected patterns for the depositing species, which are closely connected to the background concentration fields. Because grid-based observations were not available at the time of this study, a thorough quantitative model-to-measurement comparison was not possible. The site-level results for the first case study were sampled from the grid-based calculations and are therefore also indicative for adequate grid-level performance. However, a more thorough quantitative evaluation is recommended for future studies, e.g. by a grid-based model inter-comparison.

The photosynthesis and respiration schemes were evaluated by two case studies. In the first case study, the results obtained by the FACEM model were compared with CO_2 flux measurements from 26 sites participating in the CarboEurope Integrated Project. Correlations of up to $R^2 = 0.81$ indicated excellent model performance. In the second and final case study, the FACEM model was used to evaluate the effect of the 2003 European heat wave on the response of the biosphere. GPP, NPP and NEP were calculated for the years 2000–2003 and the average values for July 2000–2001 were subtracted from the average values for July 2003. The results were compared with the GPP anomaly obtained using the MOD17A2 land algorithm product derived from MODIS observations. This comparison showed that FACEM was able to reproduce the spatial distribution of the GPP anomaly well. The results of the comparison should be similar for the NPP case, because the NPP scheme implemented in the model was adopted from the MOD17A3 land algorithm. However, a comparison was not possible for this case because the MOD17A3 land algorithm provides yearly averaged values whereas the FACEM calculations were performed for the summer months only. Grid-level NEP observations were not available at the time of the study, also rendering a comparison for this case impossible. The modelled site-level fluxes were sampled from the grid-based calculations and are therefore indicative for adequate model performance. A more quantitative grid-based evaluation remains for future studies.

6. Outlook

All evaluations presented in this work indicate that FACEM is a valuable tool for future research in the field of atmosphere-canopy exchange Modelling. However, a number of shortcomings of this first version of the model will require attention during the development of future versions. For instance, incorporation of a scheme which accounts for aqueous phase chemical interaction between the acidifying and eutrophying components will be investigated. Furthermore, the simple respiration schemes introduced in this paper provide opportunities for improvement, e.g. by including a real carbon budget model and by implementing a fractionated land cover approach. The CO_2 flux estimates provided by the FACEM model provide means for atmospheric transport Modelling studies. Coupling of the FACEM model to an atmospheric transport model for prediction of site-level CO_2 concentrations will be a very logical and promising step forward.

7. Acknowledgments

We would like to thank Jørgen Brandt from NERI (Denmark) for providing all concentration and wet deposition data from the DEHM model. Also, we would like to thank Gert Jan Reinds from Alterra Green world Research (The Netherlands) for providing the CBM deposition estimates for the model-to-measurement comparisons. ECMWF is acknowledged for provision of the meteorological data. Finally, we would like to thank the CarboEurope Integrated Project for providing the CO_2 flux measurements.

References

Adiku, S. G. K., Reichstein, M., Lohila, A., Dinh, N. Q., Aurela, M. and co-authors. 2006. PIXGRO: A model for simulating the ecosystem CO_2 exchange and growth of spring barley. *Ecol. Mod.* **190**, 260–276.

Aurora, V. K. 2003. Simulating energy and carbon fluxes over winter wheat using coupled land surface and terrestrial models. *Agr. For. Met.* **118**, 21–47.

Baldocchi, D., Hicks, B. B. and Camara, P. 1987. A canopy stomatal resistance model for gaseous deposition to vegetated surfaces. *Atm. Env.* **13**, 1681–1687.

Bennet, J. H., Hill, A. C. and Dates, D. M. 1973. A model for gaseous pollutant sorption by leaves. *J. Air Pollut. Control Assoc.* **23**, 957–962.

Berry, J. A. and Farquhar, G. D. 1978. The CO_2 concentration function of C_4 photosynthesis: a biochemical model. In: *4th International Congress of Photosynthesis* (eds.D. Jall, J. Coombs and T. Goodwin), London, Biochem, Soc, pp. 119–131.

Bleeker, A., Vermeulen, A. T., Erisman, J. W., Reinds, G. J. and Vries, W. d. 2004. Critical loads and present deposition thresholds of nitrogen and acidity and their exceedances at Level II and Level I monitoring plots in Europe. Technical Report ECN-C–04-117, ECN Schoon Fossiel, The Netherlands.

Christensen, J. H. 1997. The Danish Eulerian Hemispheric Model—a three-dimensional air pollution model used for the Arctic. *Atm. Env.* **31**, 4169–4191.

Ciais, P., Reichstein, M., Viovy, N., Granier, A., Ogee, J. and co-authors 2005. Europe-wide reduction in primary productivity caused by the heat and draught in 2003. *Nature* **437**(7058), 529–533.

Claussen, M. 1990. Area-averaging of surface fluxes in a neutrally stratified, horizontally inhomogeneous atmospheric boundary layer. *Atm. Env.* **24A**, 1349–1360.

Collatz, G. J., Ball, K. T., Grivet, C. and Berry, J. A. 1991. Physiological and environmental regulation of stomatal conductance, photo synthesis and transpiration: a model that includes a laminar boundary layer. *Agr. For. Met.* **54**, 107–136.

Collatz, G. J., Ribas-Carbo, M. and Berry, J. A. 1992. Coupled photosynthesis stomatal conductance model for leaves of C_4 plants. *Aust. J. Plant Physiol.* **19**, 519–538.

Draaijers, G. P. J. and Erisman, J. W. 1995. A canopy budget model to assess atmospheric deposition from throughfall measurements. *Water Air Soil Pollut.* **85**, 2253–2258.

Draaijers, G. P. J., Erisman, J. W., Lövblad, G., Spranger, T. and Vel, E. 1998. Quality and uncertainty aspects of forest deposition estimation using throughfall, stemflow and precipitation measurements. Technical Report R98/093, TNO, The Netherlands.

Erisman, J. W. and Draaijers, G. P. J. 1995. *Atmospheric deposition in relation to acidification and eutrophication, volume 63 of Studies in Environmental Science*. Elsevier, Amsterdam, The Netherlands.

Erisman, J. W. and Wyers, G. P. 1993. Continuous measurements of surface exchange of SO_2 and NH_3; implications for their possible interaction in the deposition process. *Atm. Env.* **27A**, 1937–1949.

Erisman, J. W., van Pul, W. A. J. and Wyers, G. P. 1994. Parameterization of surface resistance for the quantification of atmospheric deposition of acidifying pollutants and ozone. *Atm. Env.* **28**, 2595–2607.

Erisman, J. W., Vermeulen, A. T., Hensen, A., Flechard, C. R., Dämmgen, U. and co-authors. 2004. Monitoring and modeling of biosphere/atmosphere exchange of gases and aerosols in europe. *Env. Poll.* **133**, 403–413.

Farquhar, G. D., Caemmerer, S. V. and Berry, J. A. 1980. A biochemical model of photosynthetic CO_2 fixation in leaves of C_3 species. *Planta* **149**, 78–90.

Finkelstein, P. L., Ellestad, T. G., Clarke, J. F., Meyers, T. P., Schwede, D. B. and co-authors. 2000. Ozone and sulfur dioxide dry deposition to forests: Observations and model evaluation. *J. of Geophys. Res.* **105**(D12), 15365–15377.

Flechard, C. R., Fowler, D., Sutton, M. A. and Cape, J. N. 1999. A dynamic chemical model of bidirectional ammonia exchange between semi-natural vegetation and the atmosphere. *Quart. J. Roy. Met. Soc.* **125**(559), 2611–2641. Part A.

Fowler, D. 1985. *Dry deposition of SO⊖ onto plant canopies*. Sulphur dioxide and vegetation. Stanford University Press, Stanford, California, USA.

Fowler, D. and Unsworth, M. H. 1979. Turbulent transfer of sulphur dioxide to a wheat crop. *Roy. Met. Soc.* **105**, 767–783.

Friedl, M. A., McIver, D. K., Hodges, J. C. F., Zhang, Z. Y., Muchoney, D. and co-authors. 2002. Global land cover mapping from MODIS: Algorithms and early results. *Rem. Sens. Env.* **83**, 287–302.

Frohn, L. M., Christensen, J. H. and Brandt, J. 2002. Development of a high resolution nested air pollution model - the numerical approach. *J. Comput. Phys.* **179**, 68–94.

Frohn, L. M., Christensen, J. H., Brandt, J., Geels, C. and Hansen, K. M. 2003. Validation of a 3-D hemispheric nested air pollution model. *Atm. Chem. Phys. Disc.* **3**, 3543–3588.

Garland, J. A. 1977. The dry deposition of sulphur dioxide to land and water surfaces. *Proc. Roy. Soc. Lond.* **A354**, 245–268.

Gauger, T., Anshelm, F., Schuster, H., Erisman, J. W., Vermeulen, A. T. and co-authors. 2003. Mapping of ecosystem specific long-term trends in deposition loads and concentrations of air pollutants in Germany and their comparison with critical loads and critical levels, Part 1: Deposition loads 1990–1999. Technical Report Final Report UBA 299 42 210, Institut für Navigation der Universität Stuttgart, on behalf of the Federal Environmental Agency (Umweltbundesamt), Berlin, Germany.

Geels, C. 2003. *Simulation the current CO⊖ content of the atmosphere: including surface fluxes and transport across the Northern Hemisphere*. Ph.D. thesis, National Environmental Research Institute, Department of Atmospheric Environment, Denmark.

Geels, C., Doney, S. C., Dargaville, S. C., Brandt, J. and Christensen, J. H. 2004. Investigating the sources of synoptic variability in atmospheric CO_2 measurements over the northern hemisphere continents - a regional model study. *Tellus* **56B**, 35–50.

Global Soil Data Task Group. 2000. Global gridded surfaces of selected soil characteristics (igbp-dis). Internet URL http://www.daac.ornl.gov from Oak Ridge National Laboratory Distributed Active Archive Center, Oak Ridge, Tennessee, USA.

Heinsch, F. A., Reeves, M., Bowker, C. F., Votava, P., Kang, S. and co-authors. 2003. Users guide: GPP and NPP (MOD17A2/A3) products NASA MODIS land algorithm.

Hicks, B. B., Hosker, R. P., Myers, T. P. and Womack, J. D. 1991. Dry deposition measurement techniques. I, design and tests of a prototype meteorological and chemical system for determining dry deposition. *Atm. Env.* **25**, 2345–2359.

Högström, U. 1998. Non dimensional Wind and temperature profiles in the atmospheric surface layer: A re-evaluation. Bound-lay. *Met*, **42**, 55–78.

Ito, A. and Oikawa, T. 2000. A model analysis of the relationship between climate perturbations and carbon budget anomalies in global terrestrial ecosystems: 1970 to 1997. *Clim. Res.* **15**, 161–183.

Joint Research Centre. 2003. Global Land Cover 2000 database (glc2000). Internet URL http://www-gvm.jrc.it/glc2000/defaultGLC2000.htm from the Joint Research Centre (European Commission), Ispra, Italy.

Jung, M., Henkel, K., Herold, M. and Ghurkina, G. 2006. Exploiting synergies of global land cover products for carbon cycle modeling. *Rem. Sens. Env.* **101**, 534–553.

Katul, G. G., Finkelstein, P. L., Clarke, J. F. and Ellestad, T. G. 1996. An investigation of the conditional sampling method used to estimate fluxes of active, reactive, and passive scalars. *J. Appl. Met.* **35**, 1835–1845.

Knorr, W. 2000. Annual and inter annual CO_2 exchanges of the terrestrial biosphere: process based simulations and uncertainties. *Glob. Ecol. Biogeo.* **9**, 225–252.

Knyazikhin, Y., Glassy, J., Privette, J. L., Tian, Y., Lotsch, A. and co-authors. 1999. MODIS leaf area index (LAI) and fraction of photosynthetically active radiation absorbed by vegetation (FPAR) product (MOD15) algorithm theoretical basis document. Internet URL http://modis.gsfc.nasa.gov/data/atbd/land˙atbd.php from the National Aeronautics and Space Administration (NASA), USA.

Liu, W. T., Katsaros, K. and Businger, J. A. 1979. Bulk parameterization of air-sea exchanges of heat and water vapor including the molecular constraints at the surface. *J. Atm. Sci.* **36**, 1722–1735.

Loveland, T. R., Reed, B. C., Brown, J. F., Ohlen, D. O., Zhu, Z. and co-authors. 2000. Development of a global land cover characteristics database and IGBP DISCover from 1-km AVHRR data. *Int. J. Rem. Sens.* **21**, 1303–1330.

Ma, J. M. and Daggupaty, S. M. 1998. Stability dependence of height scales and effective roughness lengths of momentum and heat transfer over roughness changes. *Bound. -Lay. Met.* **88**(1), 145–160.

Mahrt, L., Vickers, D., Edson, J., Sun, J. L., Hojstrup, J. and co-authors. 1998. Heat flux in the coastal zone. *Bound. -Lay. Met.* **86**(3), 421–446.

Mason, P. J. 1988. The formation of a really-averaged roughness lengths. *Quart. J. Roy. Meteor. Soc.* **114**, 399–420.

Massman, W. J. 1982. Foliage distribution in old-growth coniferous tree canopies. *Can. J. For. Res.* **12**, 10–17.

Massman, W. J. 1997. An analytical one-dimensional model of momentum transfer by vegetation of arbitrary structure. *Bound. -Lay. Met.* **83**, 407–421.

Meyers, T. P., Finkelstein, P., Clarke, J., Ellestad, T. G. and Sims, P. F. 1998. A multi layer model for inferring dry deposition using standard meteorological measurements. *J. of Geophys. Res.* **103**(D17), 22645–22661.

Philip, J. R. 1997. Blending and internal boundary-layer heights, and shear stress. *Bound. -Lay. Met.* **84**, 85–98.

Pleim, J. E., Finkelstein, P. L., Clarke, J. F. and Ellestad, T. G. 1999. A technique for estimating dry deposition velocities based on similarity with latent heat flux. *Atm. Env.* **33**(14), 2257–2268.

Potter, C. S., Randerson, J. T., Field, C. B., Matson, P. A., Vitousek, P. M. and co-authors. 1993. Terrestrial ecosystem production: a process model based on global satellite and surface data. *Glob. Biochem. Cycles* **7**(4), 811–841.

Press, W. H., Teukolsky, S. A., Vetterling, W. T. and Flannery, B. P. 1992. *Numerical Recipes in C: The art of scientific computing*. Cambridge University Press, Cambridge, UK.

Running, S. W. and Coughlan, J. C. 1988. A general model of forest ecosystem processes for regional applications, I. Hydrological balance, canopy gas exchange and primary production processes. *Ecol. Model.* **42**, 125–154.

Schaap, G. M. and Leij, F. J. 1998. Database-related accuracy and uncertainty of pedotransfer functions. *Soil Sci.* **163**, 765–779.

Schaap, G. M., Leij, F. J. and Genuchten, M. T. 2001. Rosetta: a computer program for estimating soil hydraulic parameters with hierarchical pedotransfer functions. *J. Hydrol.* **251**, 163–176.

Schuepp, P. H. 1989. Micro structure, density and wetness effect on dry deposition to foliage. *Agr. For. Met.* **47**, 179–198.

Sellers, P. J., Randall, D. A., Collatz, G. J., Berry, J. A., Field, C. B. and co-authors. 1996. A revised land surface parameterization (SiB2) for atmospheric GCMs. Part I: model formulation. *J. Clim.* **9**, 676–705.

Stull, R. B. 1988. *An Introduction to Boundary Layer Meteorology*, volume 13 of *Atmospheric and Oceanographic Sciences Library*. Kluwer Academic Publishers, Norwell.

Sutton, M. A., Wyers, G. P., Meixner, F. X., Schjorring, J. K., Kesselmeier, J. and co-authors. 1996. *Biosphere-atmosphere exchange of ammonia*. Biopshere-Atmosphere Exchange of Pollutants and Trace Substances. Springer-Verlag, New York.

van Pul, W. A. J., Potma, C., van Leeuwen, E. P., Draaijers, G. P. J. and Erisman, J. W. 1995. EDACS: European Deposition maps of Acidifying Components on a Small scale. Model description and results. Technical Report 72240105, National Institute of Public Health and Environment, Bilthoven, The Netherlands.

Verkaik, J. W. 2000. Evaluation of two gustiness models for exposure correction calculations. *J. Appl. Met.* **39**(9), 1613–1626.

Wesely, M. L. 1989. Parameterization of surface resistance to gaseous dry deposition in regional-scale numerical models. *Atm. Env.* **23**, 1293–1304.

Wieringa, J. 1986. Roughness-dependent geographical interpolation of surface wind speed averages. *Quart. J. Roy. Met. Soc.* **112**, 867–889.

Wu, Y., Sakamoto, C. M. and Botner, D. M. 1989. On the application of the CERES-Maize model to the North China plain. *Agr. For. Met.* **49**, 9–12.

Wu, Y., Brashers, B., Finkelstein, P. L. and Pleim, J. E. 2003a. A multilayer biochemical dry deposition model—1. Model formulation. *J. Geophys. Res.* **108**(D1), 4013–4013.

Wu, Y., Brashers, B., Finkelstein, P. L. and Pleim, J. E. 2003b. A multilayer biochemical dry deposition model—2. Model evaluation. *J. Geophys. Res.* **108**(D1), 4014–4014.